REPORT DOCUMENTATION PAGE		Form Approved OMB NO. 0704-0188

1. REPORT DATE (DD-MM-YYYY) 24-03-2014	2. REPORT TYPE Final Report	3. DATES COVERED (From - To) 1-Aug-2010 - 31-Jul-2015

4. TITLE AND SUBTITLE Final Report for Harvard-lead phase of Multi--Qubit Systems Based on Electron Spins in Coupled Quantum Dots Project Meeting	5a. CONTRACT NUMBER W911NF-10-1-0330
	5b. GRANT NUMBER
	5c. PROGRAM ELEMENT NUMBER 411359
6. AUTHORS Charles M. Marcus	5d. PROJECT NUMBER
	5e. TASK NUMBER
	5f. WORK UNIT NUMBER

7. PERFORMING ORGANIZATION NAMES AND ADDRESSES Harvard University 1350 Massachusetts Avenue Smith Center 600 Cambridge, MA 02138 -3846	8. PERFORMING ORGANIZATION REPORT NUMBER
9. SPONSORING/MONITORING AGENCY NAME(S) AND ADDRESS (ES) U.S. Army Research Office P.O. Box 12211 Research Triangle Park, NC 27709-2211	10. SPONSOR/MONITOR'S ACRONYM(S) ARO
	11. SPONSOR/MONITOR'S REPORT NUMBER(S) 58105-PH-MOC.32

12. DISTRIBUTION AVAILIBILITY STATEMENT

Approved for Public Release; Distribution Unlimited

13. SUPPLEMENTARY NOTES

The views, opinions and/or findings contained in this report are those of the author(s) and should not contrued as an official Department of the Army position, policy or decision, unless so designated by other documentation.

14. ABSTRACT

This is a final report for the IARPA MQCO Spin Qubits team ending in Dec. 2012, when the lead PI, Charles Marcus, moved from Harvard University to University of Copenhagen to direct the Center for Quantum Devices there. The Spin Qubits team comprises experimental and theoretical physicists, and materials scientists, working to realized gate confined multi-qubit systems in GaAs heterostructures. At the completion of the phase covered by this report, two versions of two-qubit systems were in hand, based on both singlet-triplet qubits and Loss-DiVincenzo qubits, but a successful system of three or more qubits had not been realized. The resonant exchange qubit, which

15. SUBJECT TERMS

Spin, qubit, nanoelectronics, quantum coherence, multi-qubit

16. SECURITY CLASSIFICATION OF:			17. LIMITATION OF ABSTRACT	15. NUMBER OF PAGES	19a. NAME OF RESPONSIBLE PERSON Charles Marcus
a. REPORT UU	b. ABSTRACT UU	c. THIS PAGE UU	UU		19b. TELEPHONE NUMBER +45-203-4118

Standard Form 298 (Rev 8/98)
Prescribed by ANSI Std. Z39.18

Report Title

Final Report for Harvard-lead phase of Multi--Qubit Systems Based on Electron Spins in Coupled Quantum Dots Project Meeting

ABSTRACT

This is a final report for the IARPA MQCO Spin Qubits team ending in Dec. 2012, when the lead PI, Charles Marcus, moved from Harvard University to University of Copenhagen to direct the Center for Quantum Devices there. The Spin Qubits team comprises experimental and theoretical physicists, and materials scientists, working to realized gate confined multi-qubit systems in GaAs heterostructures. At the completion of the phase covered by this report, two versions of two-qubit systems were in hand, based on both singlet-triplet qubits and Loss-DiVincenzo qubits, but a successful system of three or more qubits had not been realized. The resonant exchange qubit, which allows resonant and single-gate two-qubit operation, and also been demonstrated at the one qubit level, but not for two or more qubits.

(a) Papers published in peer-reviewed journals (N/A for none)

<u>Received</u>   <u>Paper</u>

01/22/2014 3.00 T. Hatano, T. Kubo, Y. Tokura, S. Amaha, S. Teraoka, S. Tarucha. Aharonov-Bohm Oscillations Changed by Indirect Interdot Tunneling via Electrodes in Parallel-Coupled Vertical Double Quantum Dots,
Physical Review Letters, (02 2011): 0. doi: 10.1103/PhysRevLett.106.076801

01/22/2014 4.00 Alexandr Sergeevich, Anushya Chandran, Joshua Combes, Stephen D. Bartlett, Howard M. Wiseman. Characterization of a qubit Hamiltonian using adaptive measurements in a fixed basis,
Physical Review A, (11 2011): 0. doi: 10.1103/PhysRevA.84.052315

01/22/2014 5.00 I. van Weperen, B. D. Armstrong, E. A. Laird, J. Medford, C. M. Marcus, M. P. Hanson, A. C. Gossard. Charge-State Conditional Operation of a Spin Qubit,
Physical Review Letters, (07 2011): 0. doi: 10.1103/PhysRevLett.107.030506

01/22/2014 6.00 Mark S. Rudner, Emmanuel I. Rashba. Detection of spin injection into a double quantum dot: Violation of magnetic-field-inversion symmetry of nuclear polarization instabilities,
Physical Review B, (02 2011): 0. doi: 10.1103/PhysRevB.83.073406

01/22/2014 7.00 Y. Kanai, R. S. Deacon, S. Takahashi, A. Oiwa, K. Yoshida, K. Shibata, K. Hirakawa, Y. Tokura, S. Tarucha. Electrically tuned spin–orbit interaction in an InAs self-assembled quantum dot,
Nature Nanotechnology, (07 2011): 0. doi: 10.1038/nnano.2011.103

01/22/2014 8.00 Sylvain Hermelin, Shintaro Takada, Michihisa Yamamoto, Seigo Tarucha, Andreas D. Wieck, Laurent Saminadayar, Christopher Bäuerle, Tristan Meunier. Electrons surfing on a sound wave as a platform for quantum optics with flying electrons,
Nature, (09 2011): 0. doi: 10.1038/nature10416

01/22/2014 9.00 M. S. Rudner, L. M. K. Vandersypen, V. Vuleti, L. S. Levitov. Generating Entanglement and Squeezed States of Nuclear Spins in Quantum Dots,
Physical Review Letters, (11 2011): 0. doi: 10.1103/PhysRevLett.107.206806

01/22/2014 10.00 Shuo Yang, Xin Wang, S. Das Sarma. Generic Hubbard model description of semiconductor quantum-dot spin qubits,
Physical Review B, (04 2011): 0. doi: 10.1103/PhysRevB.83.161301

01/22/2014 11.00 Diego S Acosta Coden, Rodolfo H Romero, Alejandro Ferrón, Sergio S Gomez. Impurity effects in two-electron coupled quantum dots: entanglement modulation,
Journal of Physics B: Atomic, Molecular and Optical Physics, (03 2013): 0. doi: 10.1088/0953-4075/46/6/065501

01/22/2014 12.00 Shuo Yang, S. Das Sarma. Low-noise conditional operation of singlet-triplet coupled quantum dot qubits,
Physical Review B, (09 2011): 0. doi: 10.1103/PhysRevB.84.121306

01/22/2014 13.00 Emmanuel I. Rashba. Mechanism of half-frequency electric dipole spin resonance in double quantum dots: Effect of nonlinear charge dynamics inside the singlet manifold,
Physical Review B, (12 2011): 0. doi: 10.1103/PhysRevB.84.241305

01/22/2014 14.00 M. S. Rudner, F. H. L. Koppens, J. A. Folk, L. M. K. Vandersypen, L. S. Levitov. Nuclear spin dynamics in double quantum dots: Fixed points, transients, and intermittency,
Physical Review B, (08 2011): 0. doi: 10.1103/PhysRevB.84.075339

01/22/2014 16.00 J. P. Kestner, S. Das Sarma. Proposed spin-qubit controlled-not gate robust against noisy coupling,
Physical Review A, (7 2011): 0. doi: 10.1103/PhysRevA.84.012315

01/22/2014 17.00 Xin Wang, Shuo Yang, S. Das Sarma. Quantum theory of the charge-stability diagram of semiconductor double-quantum-dot systems,
Physical Review B, (9 2011): 0. doi: 10.1103/PhysRevB.84.115301

01/22/2014 18.00 Edwin Barnes, J. P. Kestner, N. T. T. Nguyen, S. Das Sarma. Screening of charged impurities with multielectron singlet-triplet spin qubits in quantum dots,
Physical Review B, (12 2011): 0. doi: 10.1103/PhysRevB.84.235309

01/22/2014 19.00 Izhar Neder, Mark S. Rudner, Hendrik Bluhm, Sandra Foletti, Bertrand I. Halperin, Amir Yacoby.
Semiclassical model for the dephasing of a two-electron spin qubit coupled to a coherently evolving nuclear spin bath,
Physical Review B, (7 2011): 0. doi: 10.1103/PhysRevB.84.035441

01/22/2014 20.00 R. Brunner, Y.-S. Shin, T. Obata, M. Pioro-Ladrière, T. Kubo, K. Yoshida, T. Taniyama, Y. Tokura, S. Tarucha. Two-Qubit Gate of Combined Single-Spin Rotation and Interdot Spin Exchange in a Double Quantum Dot,
Physical Review Letters, (9 2011): 0. doi: 10.1103/PhysRevLett.107.146801

01/22/2014 21.00 Edwin Barnes, S. Das Sarma. Analytically Solvable Driven Time-Dependent Two-Level Quantum Systems,
Physical Review Letters, (8 2012): 0. doi: 10.1103/PhysRevLett.109.060401

01/22/2014 22.00 Xin Wang, Lev S. Bishop, J.P. Kestner, Edwin Barnes, Kai Sun, S. Das Sarma. Composite pulses for robust universal control of singlet–triplet qubits,
Nature Communications, (8 2012): 0. doi: 10.1038/ncomms2003

01/22/2014 23.00 J. I. Colless, D. J. Reilly. Cryogenic high-frequency readout and control platform for spin qubits,
Review of Scientific Instruments, (2012): 0. doi: 10.1063/1.3681195

01/22/2014 24.00 M. D. Shulman, O. E. Dial, S. P. Harvey, H. Bluhm, V. Umansky, A. Yacoby. Demonstration of Entanglement of Electrostatically Coupled Singlet-Triplet Qubits,
Science, (04 2012): 0. doi: 10.1126/science.1217692

01/22/2014 25.00 Andres A. Reynoso, Karsten Flensberg. Dephasing and hyperfine interaction in carbon nanotubes double quantum dots: Disordered case,
Physical Review B, (5 2012): 0. doi: 10.1103/PhysRevB.85.195441

01/22/2014 26.00 D. Marchenko, A. Varykhalov, M.R. Scholz, G. Bihlmayer, E.I. Rashba, A. Rybkin, A.M. Shikin, O. Rader. Giant Rashba splitting in graphene due to hybridization with gold,
Nature Communications, (11 2012): 0. doi: 10.1038/ncomms2227

01/22/2014 27.00 Luka Trifunovic, Oliver Dial, Mircea Trif, James R. Wootton, Rediet Abebe, Amir Yacoby, Daniel Loss.
Long-Distance Spin-Spin Coupling via Floating Gates,
Physical Review X, (1 2012): 0. doi: 10.1103/PhysRevX.2.011006

01/22/2014 28.00 Edwin Barnes, ?ukasz Cywi?ski, S. Das Sarma. Nonperturbative Master Equation Solution of Central Spin Dephasing Dynamics,
Physical Review Letters, (10 2012): 0. doi: 10.1103/PhysRevLett.109.140403

01/22/2014 29.00 C. Barthel, J. Medford, H. Bluhm, A. Yacoby, C. M. Marcus, M. P. Hanson, A. C. Gossard. Relaxation and readout visibility of a singlet-triplet qubit in an Overhauser field gradient,
Physical Review B, (1 2012): 0. doi: 10.1103/PhysRevB.85.035306

01/22/2014 30.00 S. Amaha, T. Hatano, H. Tamura, S. Teraoka, T. Kubo, Y. Tokura, D. G. Austing, S. Tarucha. Resonance-hybrid states in a triple quantum dot,
Physical Review B, (02 2012): 0. doi: 10.1103/PhysRevB.85.081301

01/22/2014 31.00 Dimitrije Stepanenko, Mark Rudner, Bertrand I. Halperin, Daniel Loss. Singlet-triplet splitting in double quantum dots due to spin-orbit and hyperfine interactions,
Physical Review B, (2 2012): 0. doi: 10.1103/PhysRevB.85.075416

01/22/2014 1.00 Sandra Foletti, Diana Mahalu, Hendrik Bluhm, Vladimir Umansky, Amir Yacoby. Enhancing the
Coherence of a Spin Qubit by Operating it as a Feedback Loop That Controls its Nuclear Spin Bath,
Physical Review Letters, (11 2010): 0. doi: 10.1103/PhysRevLett.105.216803

01/22/2014 2.00 S. Weiss, E. I. Rashba, F. Kuemmeth, H. O. H. Churchill, K. Flensberg. Spin-orbit effects in carbon-
nanotube double quantum dots,
Physical Review B, (10 2010): 0. doi: 10.1103/PhysRevB.82.165427

TOTAL: **30**

Number of Papers published in peer-reviewed journals:

(b) Papers published in non-peer-reviewed journals (N/A for none)

Received   Paper

TOTAL:

Number of Papers published in non peer-reviewed journals:

(c) Presentations

Number of Presentations: 0.00

Non Peer-Reviewed Conference Proceeding publications (other than abstracts):

Received   Paper

TOTAL:

Number of Non Peer-Reviewed Conference Proceeding publications (other than abstracts):

Peer-Reviewed Conference Proceeding publications (other than abstracts):

<u>Received</u>   <u>Paper</u>

TOTAL:

Number of Peer-Reviewed Conference Proceeding publications (other than abstracts):

(d) Manuscripts

<u>Received</u>   <u>Paper</u>

TOTAL:

Number of Manuscripts:

Books

<u>Received</u>   <u>Paper</u>

TOTAL:

Patents Submitted

Patents Awarded

Awards

Graduate Students

NAME	PERCENT_SUPPORTED	Discipline
Brian Schultz	1.00	
Borzoyeh Shojaei	1.00	
Jason Kester	1.00	
James Colless	1.00	
Alice Mahoney	1.00	
Xanthe Croot	1.00	
James Medford	1.00	
Prashant Kumar	1.00	
FTE Equivalent:	**8.00**	
Total Number:	**8**	

Names of Post Doctorates

NAME	PERCENT_SUPPORTED
Hong Lu	1.00
Ed Barnes	1.00
Floris Braakman	1.00
Javad Shabani	1.00
Ferdinand Kuemmeth	1.00
Hendrik Bluhm	1.00
Jelena Klinovaja	1.00
Tomohiro Otsuka	1.00
Sylvain Blanvillain	1.00
Andres Reynoso	1.00
FTE Equivalent:	**10.00**
Total Number:	**10**

Names of Faculty Supported

NAME	PERCENT_SUPPORTED	National Academy Member
Chris Palmstrom	1.00	
Sankar Das Sarma	1.00	
Lieven Vandersypen	1.00	
Bertrand Halperin	1.00	No
Charles Marcus	1.00	
Amir Yacoby	1.00	
Daniel Loss	1.00	
Seigo Tarucha	1.00	
David Reilly	1.00	
Stephen Bartlett	1.00	
Andrew Doherty	1.00	
FTE Equivalent:	**11.00**	
Total Number:	**11**	

Names of Under Graduate students supported

NAME	PERCENT_SUPPORTED
FTE Equivalent:	
Total Number:	

Student Metrics

This section only applies to graduating undergraduates supported by this agreement in this reporting period

The number of undergraduates funded by this agreement who graduated during this period: 0.00

The number of undergraduates funded by this agreement who graduated during this period with a degree in science, mathematics, engineering, or technology fields:······ 0.00

The number of undergraduates funded by your agreement who graduated during this period and will continue to pursue a graduate or Ph.D. degree in science, mathematics, engineering, or technology fields:······ 0.00

Number of graduating undergraduates who achieved a 3.5 GPA to 4.0 (4.0 max scale):...... 0.00

Number of graduating undergraduates funded by a DoD funded Center of Excellence grant for Education, Research and Engineering:...... 0.00

The number of undergraduates funded by your agreement who graduated during this period and intend to work for the Department of Defense 0.00

The number of undergraduates funded by your agreement who graduated during this period and will receive scholarships or fellowships for further studies in science, mathematics, engineering or technology fields: 0.00

Names of Personnel receiving masters degrees

NAME

Total Number:

Names of personnel receiving PHDs

NAME

Total Number:

Names of other research staff

NAME	PERCENT_SUPPORTED
Jessica Martin	1.00
FTE Equivalent:	**1.00**
Total Number:	**1**

Sub Contractors (DD882)

1 a. University of Sydney

1 b. A28 Physics Road

Sydney   2006

Sub Contractor Numbers (c):
Patent Clause Number (d-1):
Patent Date (d-2):
Work Description (e):
Sub Contract Award Date (f-1):
Sub Contract Est Completion Date(f-2):

1 a. University of Sydney

1 b. Camperdown Campus

Sydney   NSW 2006   2006

Sub Contractor Numbers (c):
Patent Clause Number (d-1):
Patent Date (d-2):
Work Description (e):
Sub Contract Award Date (f-1):
Sub Contract Est Completion Date(f-2):

1 a. University of Sydney

1 b. School Of Physics, A28

Sydney 2006

Sub Contractor Numbers (c):
Patent Clause Number (d-1):
Patent Date (d-2):
Work Description (e):
Sub Contract Award Date (f-1):
Sub Contract Est Completion Date(f-2):

1 a. University of Sydney

1 b. A28 Physics Road

Sydney 2006

Sub Contractor Numbers (c):
Patent Clause Number (d-1):
Patent Date (d-2):
Work Description (e):
Sub Contract Award Date (f-1):
Sub Contract Est Completion Date(f-2):

1 a. University of California - Santa Barbara

1 b. 3227 Cheadle Hall

3rd floor, MC 2050

Santa Barbara   CA   931062050

Sub Contractor Numbers (c):
Patent Clause Number (d-1):
Patent Date (d-2):
Work Description (e):
Sub Contract Award Date (f-1):
Sub Contract Est Completion Date(f-2):

---

1 a. University of California - Santa Barbara

1 b. Office Of Research

Cheadle Hall, Room 3227

Santa Barbara   CA   931062050

Sub Contractor Numbers (c):
Patent Clause Number (d-1):
Patent Date (d-2):
Work Description (e):
Sub Contract Award Date (f-1):
Sub Contract Est Completion Date(f-2):

---

1 a. University of Maryland - College Park

1 b. Office of Research Administration

3112 Lee Building

College Park   MD   207425141

Sub Contractor Numbers (c):
Patent Clause Number (d-1):
Patent Date (d-2):
Work Description (e):
Sub Contract Award Date (f-1):
Sub Contract Est Completion Date(f-2):

---

1 a. University of Maryland - College Park

1 b. 3112 Lee Building

College Park   MD   207425141

Sub Contractor Numbers (c):
Patent Clause Number (d-1):
Patent Date (d-2):
Work Description (e):
Sub Contract Award Date (f-1):
Sub Contract Est Completion Date(f-2):

---

1 a. Delft Institute of Technology

1 b. Postbus 5

Delft   AA   2600

Sub Contractor Numbers (c):
Patent Clause Number (d-1):
Patent Date (d-2):
Work Description (e):
Sub Contract Award Date (f-1):
Sub Contract Est Completion Date(f-2):

1 a. University of Basel   1 b. Petersplatz 1

                                                        Basel   XX   4003

Sub Contractor Numbers (c):
Patent Clause Number (d-1):
Patent Date (d-2):
Work Description (e):
Sub Contract Award Date (f-1):
Sub Contract Est Completion Date(f-2):

---

1 a. Oxford Instruments   1 b. Tubney Wood

                                                        Abington   UK   00000

Sub Contractor Numbers (c):
Patent Clause Number (d-1):
Patent Date (d-2):
Work Description (e):
Sub Contract Award Date (f-1):
Sub Contract Est Completion Date(f-2):

---

1 a. University of Tokyo   1 b. Department of Physics

                                                        Tokyo   AA   00000

Sub Contractor Numbers (c):
Patent Clause Number (d-1):
Patent Date (d-2):
Work Description (e):
Sub Contract Award Date (f-1):
Sub Contract Est Completion Date(f-2):

Inventions (DD882)

Scientific Progress

Technology Transfer

ARO Final Report - Harvard Lead Phase

Statement of the problem studied: During the Harvard-lead Phase, the ARO-IARPA MQCO team investigated three types of spin qubits, both realized in coupled, gate-defined quantum dots in high-mobility GaAs heterostructures. The first is the Loss-DiVincenzo (LD) qubit, where a single electron spin defines the logical qubit. The second is the singlet-triplet (ST) qubit, where the two zero-spin-projection subspace of two spins in two dots, the singlet and m=0 triplet—constitute the qubit. The third is the exchange-only (EO) qubit comprising three spins, where exchange between electrons 1 and 2 gives one rotation axis, and exchange between 2 and 3 gives a second axis. The Bloch spheres for the three qubits are shown in Fig.1. Measurements are carried out by fast charge sensing using proximal charge detectors or dispersive charge read-out. Conversion of spin states to charge readout takes advantage of the Pauli principle preventing double occupancy of the ground orbital state of a dot. Experiment is performed in a dilution refrigerator at millikelvin temperatures.
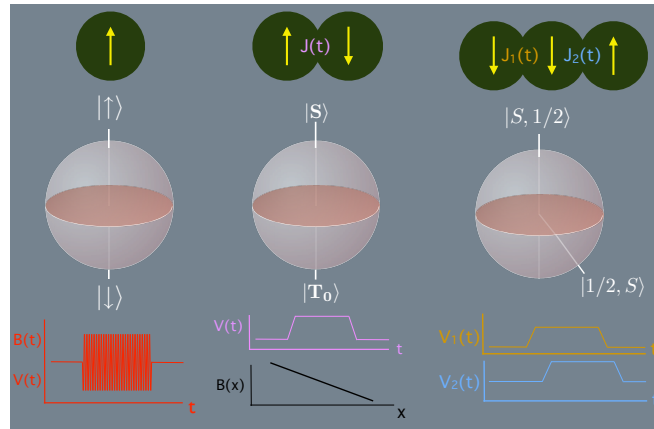
Fig. 1. Bloch spheres and elementary spin representations for Loss-Divincenzo (LD), Singlet-triplet (ST) and Exchange Only (EO) qubits [from left to right]. The experimental needs for qubit control are illustrated below.

The reason for all of these different versions is that the development of the qubit itself is under development, given the early stage of the technology. ST qubits are the most advanced, EO qubits are the least. All have some advantages and some weaknesses.

Pulses for initialization and manipulation are applied to electrostatic gates using room-temperature arbitrary waveform generators (AWG's). For the LD qubit, single qubit rotations are done using electric dipole spin resonance (EDSR), which requires pulsed microwaves at frequencies roughly from 1 to 20 GHz. Charge state readout uses fast amplifiers, located either at the 4K stage of the refrigerator or room temperature. For ST and EO qubits, ideally square voltage pulses on gates are used. Circuit boards for bring GHz-scale pulses onto the chip have been the focus of considerable effort during this period. An example of circuit board developed during the Harvard-lead period is shown in Fig. 3. All measurements are carried out at low temperature (mK). A new cryogen-free refrigerator is shown in Fig. 4.
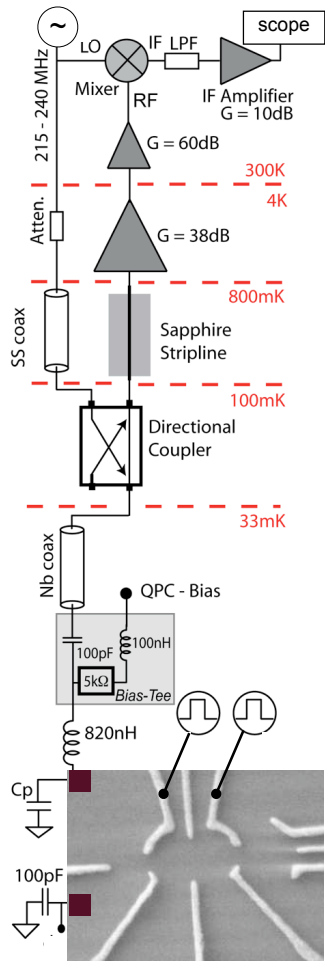
Fig. 2. Fast readout electronics based on high-Q resonant circuit.
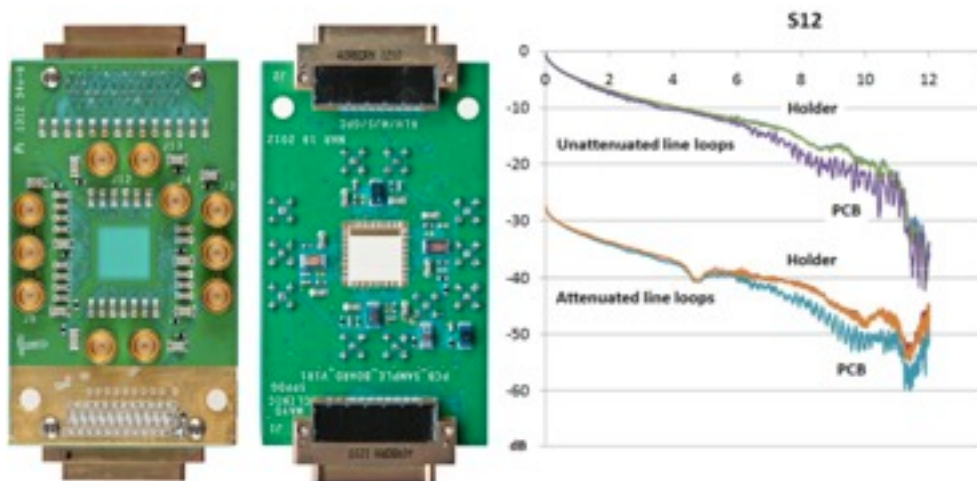
Fig. 3. High-bandwidth circuit boards designed for spin qubits.

Fig. 4. A cryogen-free dilution refrigerator (opened).

Summary of Accomplishments

Summary of Accomplishments	Measurement	Results	Notes
3.1 Single LD Qubit			See Sec. 3.1
	T_1 Measurement	See Fig. 3.1.3	T1 left = 4.9 ± 1.7 ms T1 right = 3.8 ± 0.7 ms
	Full Control	See Fig. 3.1.4	
	State Tomography		In progress
3.2 Two LD Qubits			
	Universal Entangling Gate definition	See Figs. 3.2.1-3.2.2	Exchange gate: sqrt(SWAP)
	State Tomography and duration of gate	In progress	
LD Readout		P left 0 = 0.950 ± 0.5 P left 1 = 0.780 ± 4 P right 0 = 0.957 ± 0.4 P right 1 = 0.777 ± 0.9	See notes in Sec. 3.2
	P_{00}	0,95	
	P_{01}	0,05	
	P_{10}	0,78	
	P_{11}	0,22	
	Detection Time	~ 2 ms for tunneling event	
	Detection Fidelity (ability to distinguish between the two qubit states)	Upper bound for the fidelity after a quarter period (sqrt swap), is the fourth root of 0.977, ~ 0.994.	
3.3 Single ST Qubit			See Sec. 3.3
	T_1 Measurement	1-10 ms (See Fig. 3.3.2)	
	State Tomography and duration for gate	Fidelity 0.97 typical gate time ~ 10 ns	See Fig. 3.3.6
	Process Tomography for ($\pi/2$) gate	Fidelity 95%	See Figs. 3.3.8 and 3.3.9
3.4 Two ST Qubits			See Sec. 3.4

Summary of Accomplishments	Measurement	Results	Notes
	CPhase(π)	Include Truth Table	
ST Readout			See Sec. 3.4
	P_{00}	0,99	See Fig. 3.3.5
	P_{01}	0,03	See Fig. 3.3.5
	P_{10}	0,01	See Fig. 3.3.5
	P_{11}	0,97	See Fig. 3.3.5
	Detection Time	0.8 μs	
	Detection Fidelity (ability to distinguish between the two qubit states)	0.98	
3.5 Single EO Qubit			See Sec. 3.5
	Readout Fidelty	Singlet Fidelity 0.96 Triplet Fidelity 0.90 See Fig. 3.5.2	
	State Tomography	Average fidelity = 0.75 See Fig. 3.5.3	

3.1. Single LD Qubit

T1 measurement
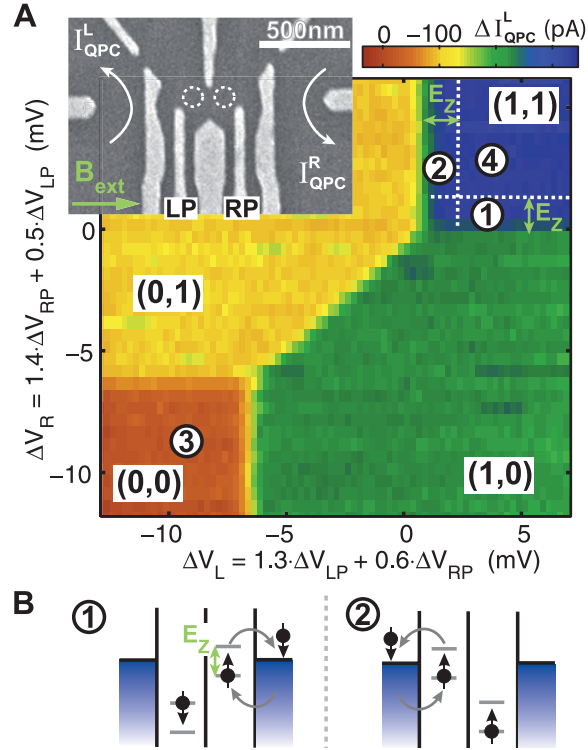
Fig. 3.1.1 (A) Charge stability diagram, with charge-sensing current I^L_{QPC} shown in color scale as a function of voltages applied to gates LP and RP (a background plane has been subtracted). The occupation in the left and right dots is indicated by numbers in brackets. (Inset) Scanning electron micrograph of a device similar to the one used in our experiment. Gates LP and RP are connected to high-frequency lines via bias-tees. The direction of B_{ext} is indicated. (B) Electrochemical potential diagrams showing the double-dot configuration in the two read-out stages [positions (1) and (2) in (A)]. Tunnel events that occur for a ↓↓ state are indicated. From Ref. [1].

3.1. Single LD Qubit
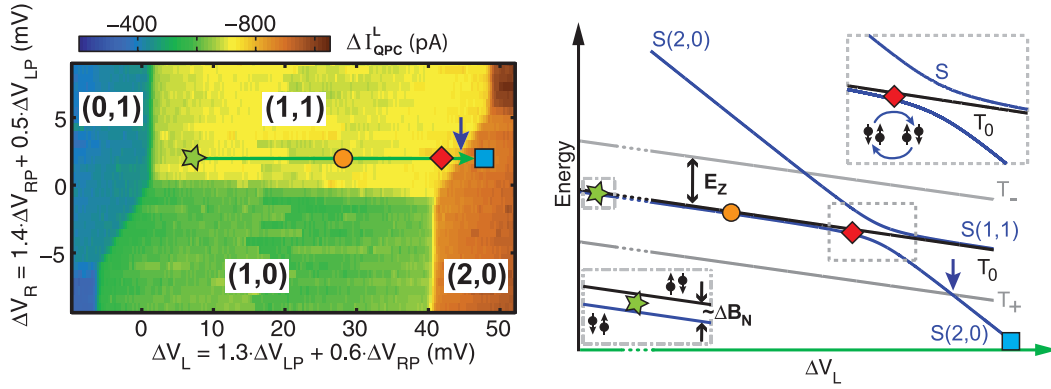
Fig. 3.1.2 (Left) Pulse sequence shown on charge stability diagram including the (2,0) charge region. (Right) Energy diagram showing the pulse sequence. From Ref. [1].
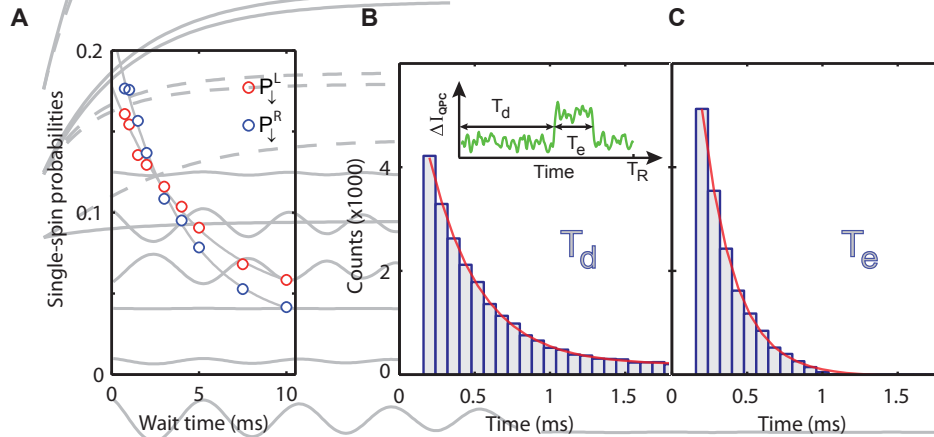
Fig. 3.1.3 (A) Single dot relaxation as a function of wait time. Grey lines are fits to $\rho \cdot e^{-t/T1} + \alpha$. (B) Histogram showing the distribution of the time T_d it takes a spin-down electron to tunnel out. The red line is an exponential fit from which we can find the decay rate. Inset: real time trace of one of the read out stages indicating the detection time (T_d) and the event time (T_e). (C) Histogram showing the distribution of the time T_e it takes a spin-up electron to tunnel back into the empty dot. The red line is an exponential fit from which we can extract the decay rate. From Supplemental Material to Ref. [1].

3.1. Single LD Qubit

Full Qubit Control
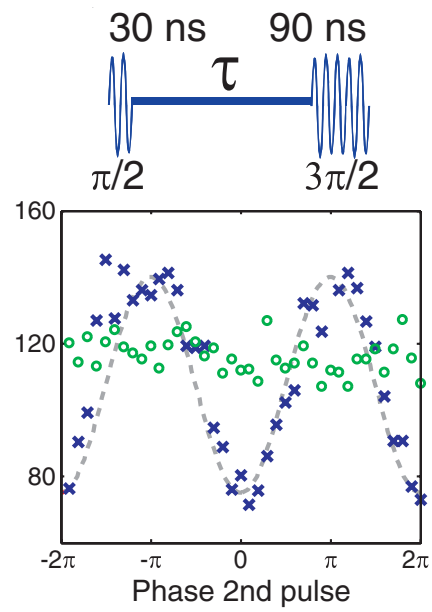
Fig. 3.1.4 Ramsey signal as a function of the relative phase between the two rf bursts for τ = 10ns (crosses) and 150 ns (circles). Gray dashed line is a best fit of a cosine to the data. From [2].

3.2 LD Two Qubit Operation

**Entangling operation: Exchange operation on two LD qubits.**
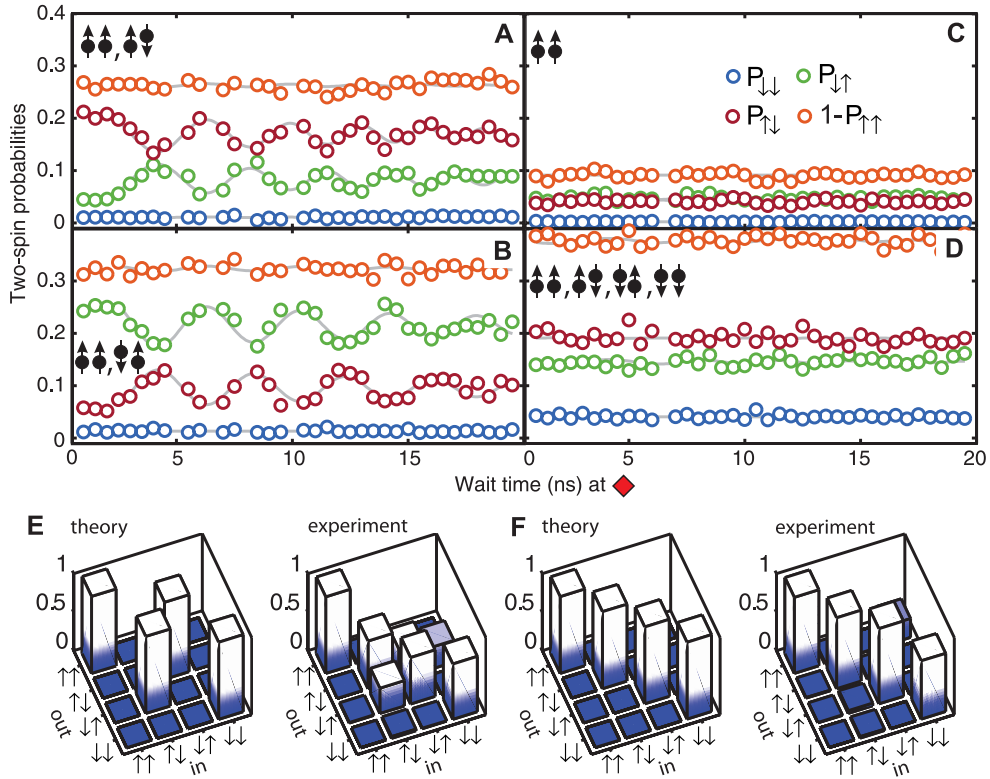
Fig. 3.2.1 (A to D) Two-qubit exchange gate on a full set of input states. The four panels correspond to four different mixtures of initial states, as indicated, taken with otherwise identical settings. Again, spin-down injection probabilities are below 50%. Gray lines are fits to damped oscillations, including a correction for pulse imperfections. We first fit $P_{\uparrow\downarrow}$ in (A) and $P_{\downarrow\uparrow}$ in (B) and allow only the amplitude and offset of the oscillations to change for the other probabilities in the respective panel. In (C) and (D), we use the fit parameters of (A) and allow only amplitude and offset to change. The oscillations in (A) and (B) run out of phase with each other for longer wait times. We attribute this to subtle distortions of the pulses arriving at the sample due to the bias tees (22). (E and F) Visualized theoretical and experimental truth tables for a π rotation and a 2π rotation of the exchange oscillation. From Ref. [1].

3.2 LD Two Qubit Operation

## Entangling operation: Exchange gate with single qubit operations
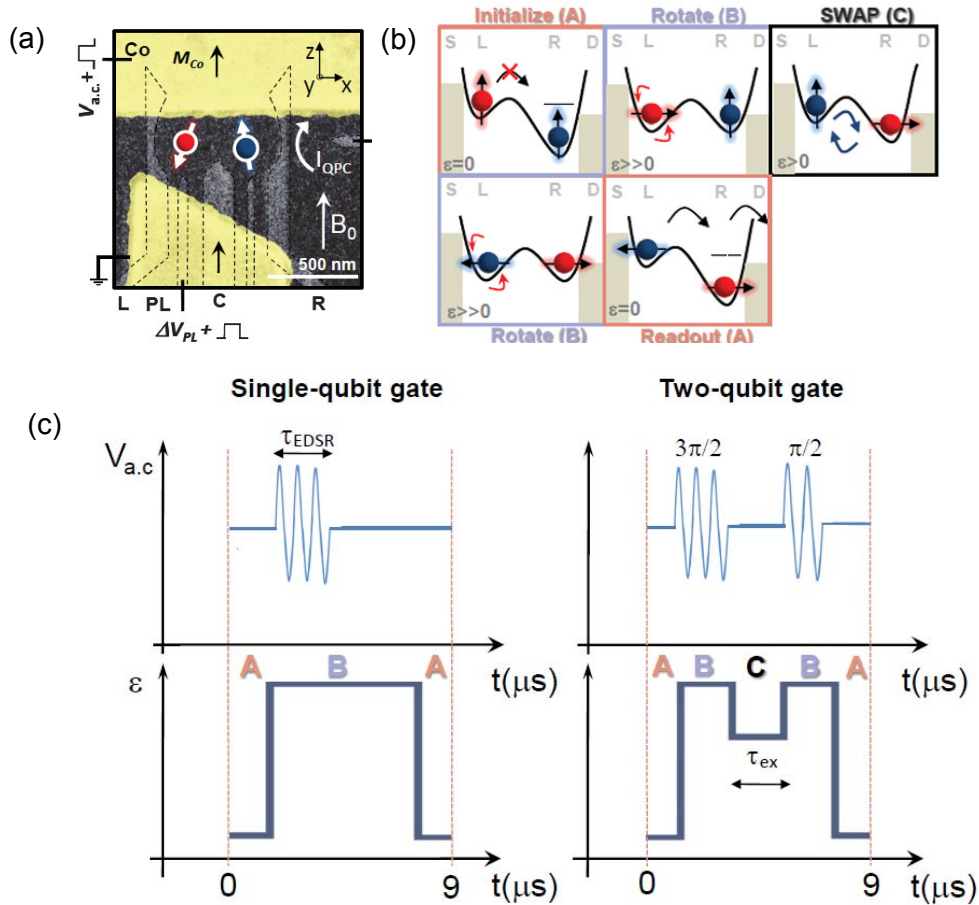
Fig. 3.2.2. (a) Scanning electron microscopy image of the device fabricated on top of an AlGaAs/GaAs heterostructure showing the Ti=Au gates (light gray) and the split cobalt (Co) magnet (yellow) separated from the gate contacts by a calixarene layer. Gates R (right) and L (left) control N_R and N_L; C (center) controls the interdot tunnel coupling t. Fast voltage pulses are applied to the Co and PL gates. A MW voltage Vac is applied to the upper part of the magnet. G_{QPC} is measured by modulating the P_L gate voltage V_{PL}. (b) Cycle of the two qubit gate operation with source (S), drain (D), left (L), and right (R) QDs. From Ref. [3]. (C) Pulsing voltages to demonstrate the quantum operation of the single-qubit and two- qubit gate. The voltage pulses are applied to switch between: A→B→A (controlled single-spin rotations, left panel) and A→B→C→B→A (quantum circuit comprising controlled single spin rotations and exchange operation, right panel). The control cycle for the controlled single spin rotations consists of initialization (A), spin rotation (B) and readout (A). The control cycle for the multiple-qubit gate consists of initialization (A), spin rotation (θ=3π/2) (B), spin exchange or "SWAP" (C), spin rotation (θ =π/2) (B) and singlet readout (A).

3.3 Single ST Qubit

T1 Relaxation
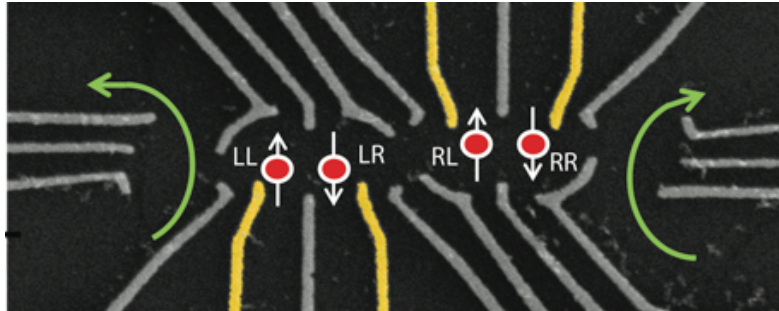


Fig. 3.3.1 Capacitively Coupled two-ST qubit device. From Ref. [4].
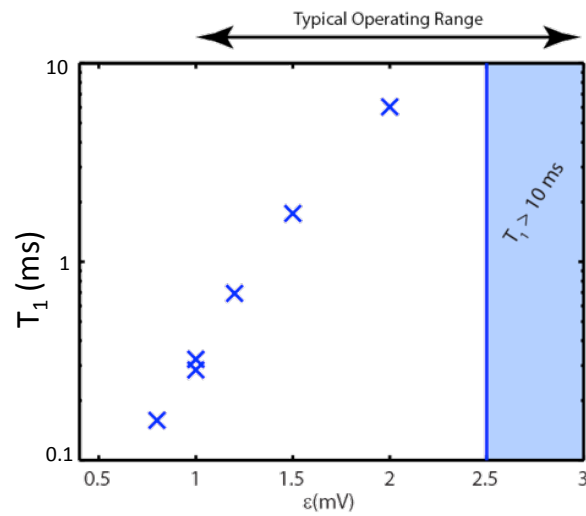
Fig. 3.3.2 Qubit relaxation time T1 as a function of detuning into the measurement position.

3.3 Single ST Qubit

Definition of Fidelity

In order to quantitatively interpret sensor values for state tomography, it is important to precisely determine the RF sensor response that corresponds to a $|S\rangle$ or a $|T_0\rangle$ state. Because the state preparation is imperfect, it is in general difficult to accurately measure these values experimentally. To provide exact calibrations for $|S\rangle$ and $|T_0\rangle$, we exploit the fact that our sensor is capable of single shot readout. Histograms of sensor values for typical measurements yield a double-peaked curve- one peak corresponds to $|T_0\rangle$ and one to $|S\rangle$ (Fig. 3.3.3). In order to calibrate the sensor we first measure T_1 at the measurement point by preparing a state that is majority $|T_0\rangle$ (done with a π-pulse around the x-axis) and fitting the sensor signal to a decaying exponential function of time elapsed during measurement (Fig. 3.3.3.a). We note that the measured value of T_1 is a strong function of the power of the RF excitation used to read the conductance of the sensing QD. With prior knowledge of T_1, we use a procedure similar to that described in Barthel et. al (14) to optimize the measurement time given our signal to noise ratios and T_1. This process is repeated several times per day to check for drift. We recalibrate the sensor signals that correspond to $|S\rangle$ and $|T_0\rangle$ for each dataset (typically 10 minutes of acquisition time). For each set, we prepare a histogram of all observed sensor values. The presence of several reference measurements in each dataset guarantees that there will be a significant fraction of both $|S\rangle$ and $|T_0\rangle$. We then fit this double peaked curve to an analytic expression corresponding to a weighted sum of two Gaussians with some filling in due to T_1 decay during measurement (Fig. 3.3.3.b, purple line) as in ref. 14. From this, we extract the expected sensor distribu$|T_0\rangle$tions for $|S\rangle$ and $|T_0\rangle$ (blue and red lines in Fig. S1b, respectively), as well as the fractions of $|S\rangle$ and $|T_0\rangle$ present. The centers of the two distributions correspond to the sensor signals that will be measured for pure $|S\rangle$ and pure $|T_0\rangle$, and using these values we can accurately scale the tomography data. We note that this procedure is insensitive to the percentages of $|S\rangle$ and $|T_0\rangle$. In our state tomography only expectation values are needed, so the single-shot capability of our readout is not necessary beyond this calibration. Nonetheless, we note that for the data presented, we measured readout fidelities of 97% and 98% for the left and right qubits, respectively.
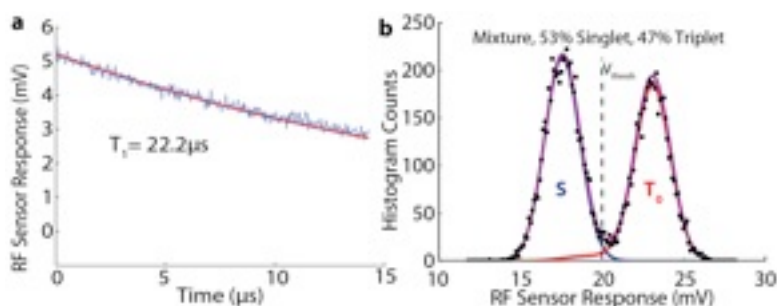

Fig. 3.3.3. Singleshot Readout: a, The difference in sensor signal between $|S\rangle$ and $|T_0\rangle$ is fit to a decaying exponential to determine T_1, which is used in calibration of sensor values. b, The histograms of a mixture of $|S\rangle$ and $|T_0\rangle$ states used to calibrate the sensor values. If we choose a threshold V_{thresh} to distinguish between $|S\rangle$ and we see a readout fidelity of 97%. Purple: fit to noisy distribution including T_1 decay from $|T_0\rangle$ to $|S\rangle$. The deduced distribution for $|S\rangle$ (blue) is a Gaussian, while that for $|T_0\rangle$ (red) has a tail due to T_1 decay.

3.3 Single ST Qubit

Crosstalk considerations
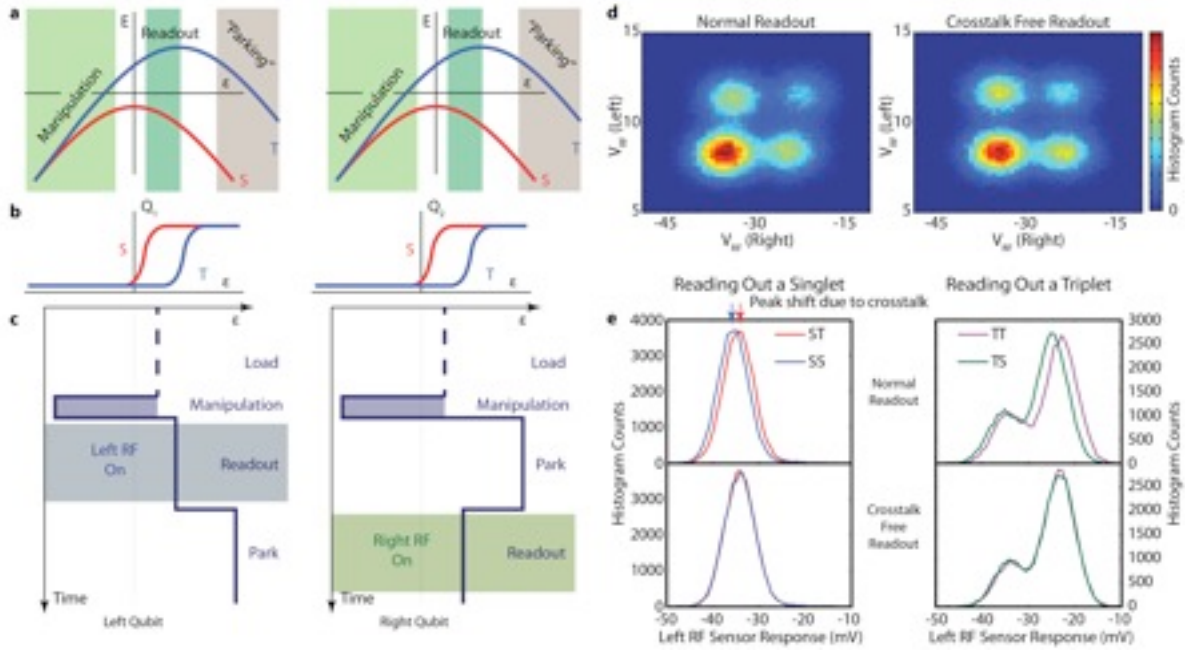
Fig. 3.3.4. a, A schematic of the energy diagram as a function of ε that describes the two qubits and shows the regions of ε where different operations are carried out. b, A schematic of the signal from the RF charge sensor as a function of ε for the two qubits. This signal reflects the charge distribution of the two qubit states. For large positive ε there is a region where $|S\rangle$ and $|T_0\rangle$ have the same sensor signal (charge distribution), which is the foundation of the crosstalk-free readout scheme. c, A schematic of the readout scheme that eliminates crosstalk. First, the left qubit is read while the right qubit is ``parked'' in (0,2), and then the right qubit is read while the left qubit is "parked" in (0,2). d, A two dimensional histogram of the RF sensor responses without (left panel) and with (right panel) this crosstalk-free readout scheme. e, Histograms of sensor values without (top) and with (bottom) the crosstalk-free readout. Without the crosstalk-free readout the sensor signal of one qubit depends on the state of the other qubit.

3.3 Single ST Qubit - Readout Fidelity

Integration time = 800ns
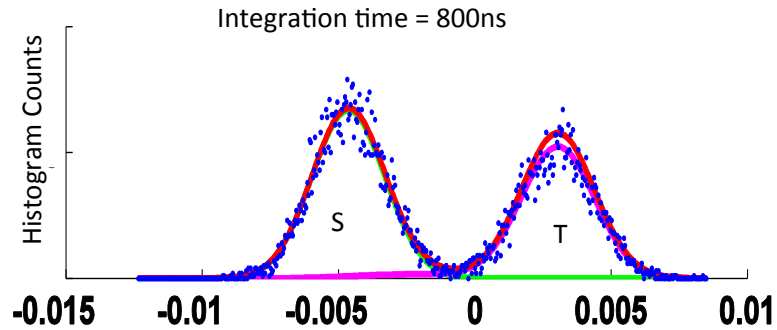
Probability of measuring S if we had a S= 0.992

Probability of measuring S if we had a T= 0.027

Probability of measuring T if we had a S= 0.008

Probability of measuring T if we had a T= 0.973

Fig. 3.3.5 We prepare |S> many times and measure it. We also prepare |T> many times (using prepared hyperfine gradient dBz) and measure. We fit the sensor signal to a two peaked Gaussian, allowing for T1 (measured independently) decay, and allowing for imperfect preparation of |T> (i.e. some of the states that we initially assumed to be |T> were actually |S> for instance because of a bad dBz pulse). We then pick the sensor threshold that optimally discriminates between a hypothetical population of perfect singlets from perfect triplets and calculate error probabilities from the measured distributions.

3.3 Single ST Qubit

Single ST qubit state tomography
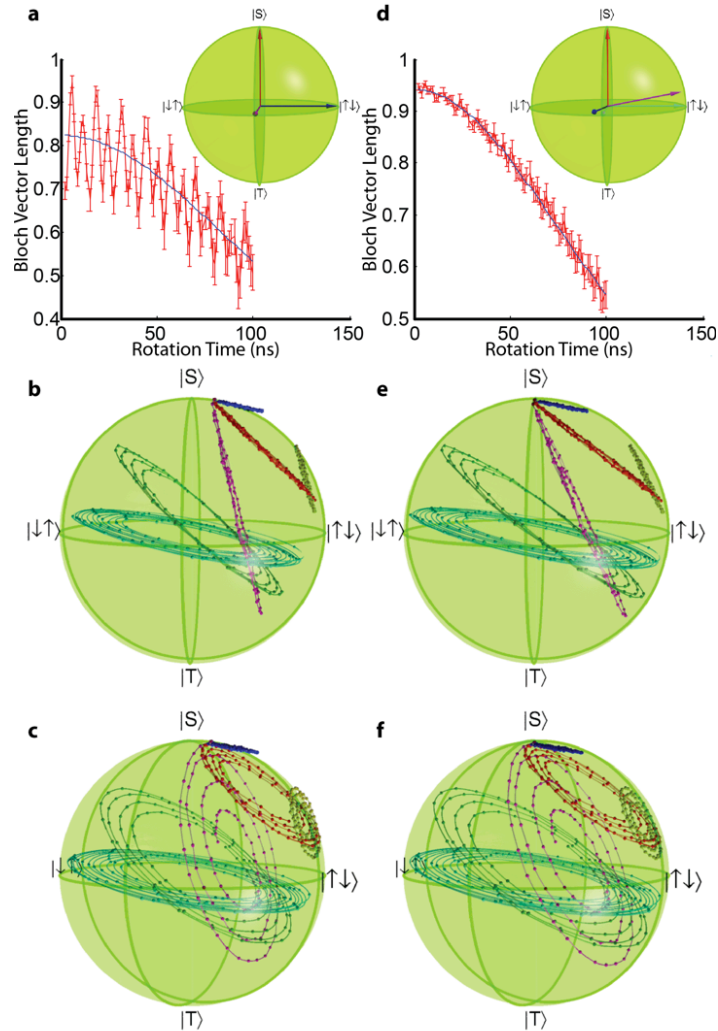
Fig. 3.3.6 Calibrated versus uncalibrated state tomography: a, Data taken to calibrate the tomography shows ripples in the length of the Bloch vector if we assume that the tomography projects the quantum state on to Cartesian axes (inset). b-c, The paths around the Bloch sphere for the different evolutions that are used for tomography calibration. If the tomography is assumed to project on to the Cartesian axes there are points that lay outside the Bloch sphere, and the pure states are not at the north pole, which is indicative of flawed state tomography. d, The ripples in the length of the Bloch vector are diminished (compared to panel a) if the axes deduced from state tomography (inset) are used. e-f, The paths around the Bloch sphere for the different evolutions that are used for state tomography. When the correct axes are used, all the points lie inside the Bloch sphere and the pure are at the north pole.

3.3 Single ST Qubit

Single qubit process tomography
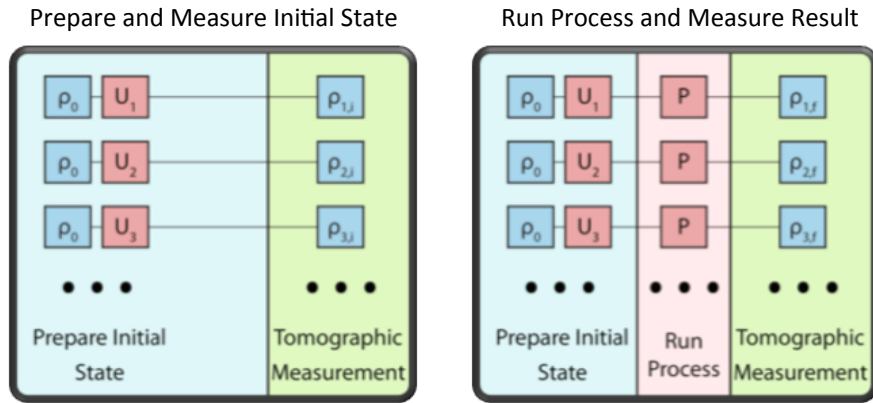
Fig. 3.3.7 Process tomography of a single ST qubit uses 6 initial states. Processes are repeated many times, then Chi matrices are calculated which maximize the likelihood of an observed process.
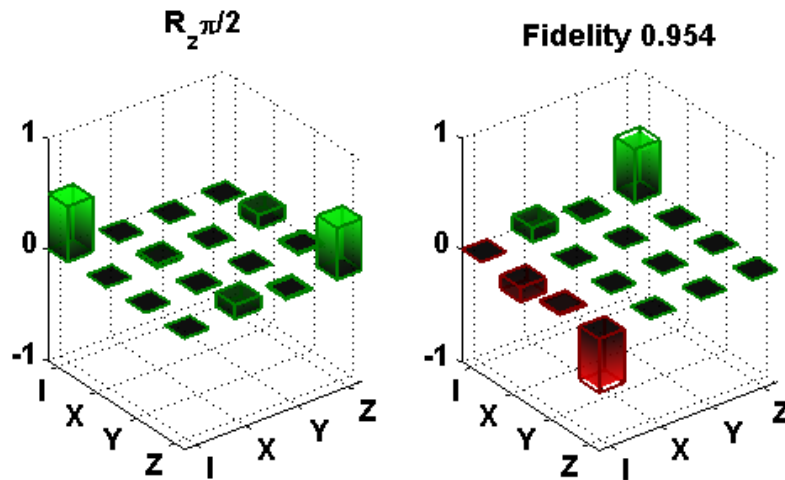

Fig. 3.3.8 For tuning up a Clifford set we use a set of axes that is rotated slightly compared to the ST, up-down, axes because rotations around the z and x axes are challenging. Shown is the $\pi/2$ process tomography, tuned around the new z-axis, which is the axis [.26, .03, .97] instead of [0,0,1]. Using the procedure above, we calibrate a $\pi/2$ rotation around this axis and find a process fidelity of 95%. Shown is the Chi matrix for this process in the normal S-T, up-down/down-up, basis.

3.3 Single ST Qubit

Name	Process	Fidelity	Times	Axis	dephasing
Z-π/2	J	.99	2ns	[.28 .03 .96]	.99
Z-π	JJ	.95	3ns	[.22 -.04 .97]	.98
Z-3π/2	JJJ	.97	5ns	[.31 -.1 .95]	.98
Z-π/4	J-π/4	.96	2ns	[.39 -.05 .92]	.94
X-π/2	HJH	.90	10-2-10 (22ns)	[.97 .14 -.2]	
X-π	HJJH	.94	10-3-10ns (23ns)	[.94 .22 -.24]	
X-3π/2	HJJJH	.79	10-5-10ns (25ns)	[.97 .21 -.12]	
Y-π/2	JJH	.91	3-10 (13ms)	[.19 -.97 .13]	
Y-π	HJJHJJ	.96	10-3-10-3 (25ns)	[-.4 .89 .21]	
Y-3π/2	HJJ	.95	10-3 (13ns)	[-.19 .97 -.13]	

Fig. 3.3.9 Process Fidelity for Clifford gate set indicating the axes used for rotation. J is π/2 rotation around the designated z axis; H is Hadamard gate. Note example fidelities are in the range > 0.94.
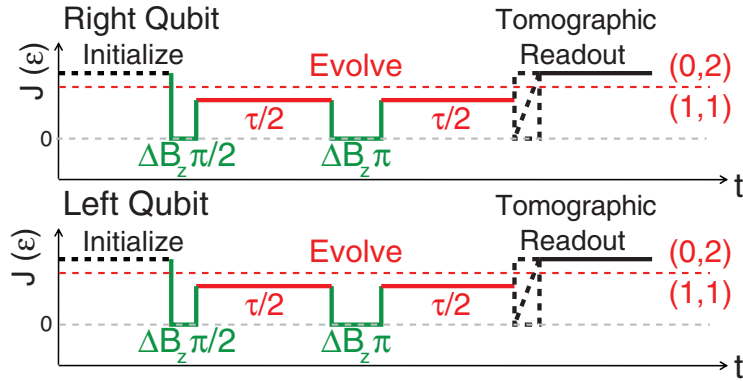
Fig. 3.4.1 The two-qubit pulse sequence used to entangle the qubits: initialize each qubit in the singlet state; perform a π/2 rotation around the x axis; allow the qubits to evolve under exchange for a time t/2; perform a π rotation around the x axis, thereby decoupling the qubits from the environment but not each other; evolve under exchange for t/2; and perform state tomography to determine the resulting density matrix. From Ref. [4].
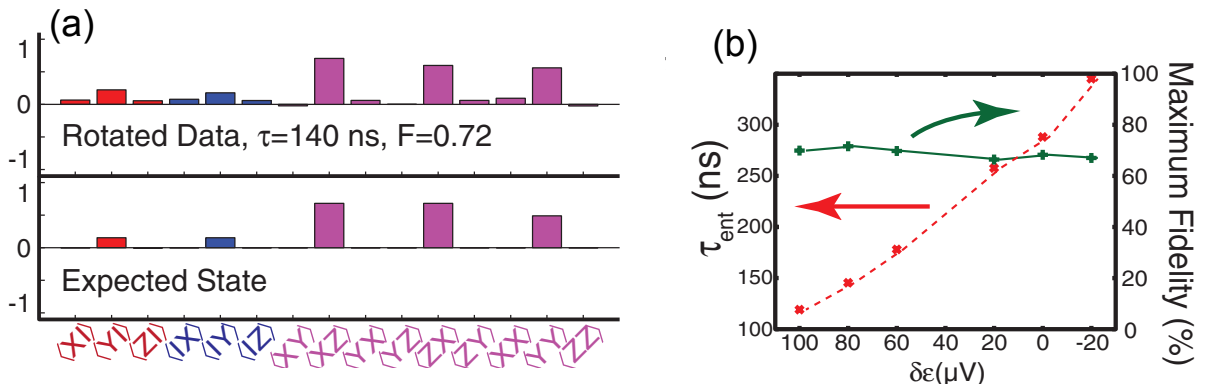

Fig. 3.4.2 (a) The elements of the Pauli set of the measured and expected states for τ = 140 ns (maximum Bell state fidelity 0.72). (b) Maximum fidelity and time for the entangling operation. From Ref. [4].

18

3.5 Single EO Operations
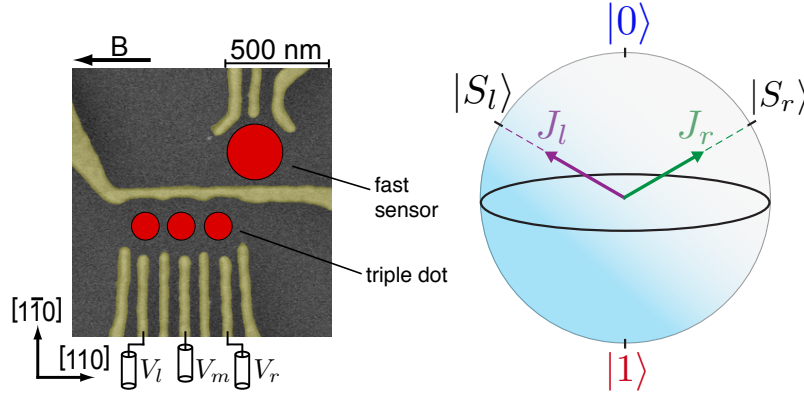
Fig. 3.5.1 Three electrons with controlled coupling 1-2 and 2-3 form an exchange only qubit [6]. The two control axes are indicated on the Bloch sphere.
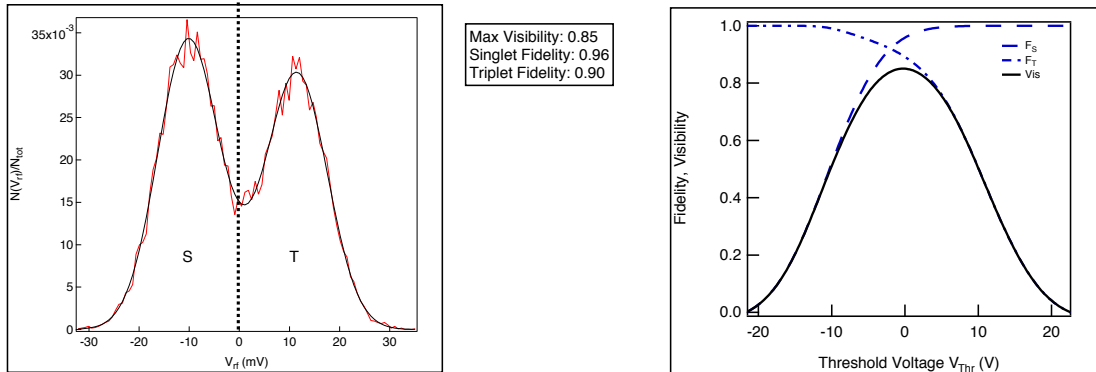

Fig. 3.5.2 Readout fidelity of EO qubit. Singlet fidelity is 0.96. Triplet fidelity is 0.90, lowered because of T_1 processes.

3.5 Single EO Operations

state tomography
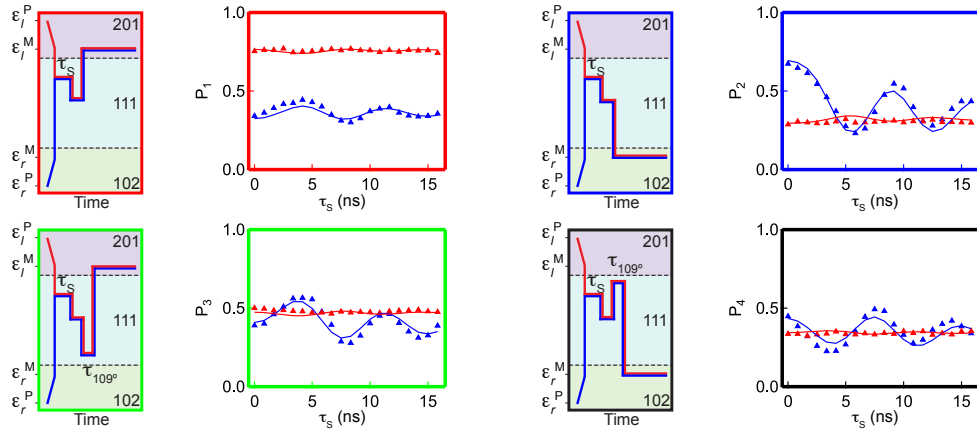
probabilities in non-orthogonal basis

$$P_1(\rho) = \mathrm{Tr}[\hat{E}_1 \rho]$$
$$P_2(\rho) = \mathrm{Tr}[\hat{E}_2 \rho]$$
$$P_3(\rho) = \mathrm{Tr}[\hat{E}_3 \rho]$$
$$P_4(\rho) = \mathrm{Tr}[\hat{E}_4 \rho]$$

five density matrices

$$\rho_1 = |S_l\rangle\langle S_l|$$
$$\rho_2 = |S_r\rangle\langle S_r|$$
$$\rho_3 = \left|\hat{R}_r S_l\right\rangle\left\langle \hat{R}_r S_l\right|$$
$$\rho_4 = \left|\hat{R}_l S_r\right\rangle\left\langle \hat{R}_l S_r\right|$$
$$\rho_5 = |mixed\rangle\langle mixed|$$
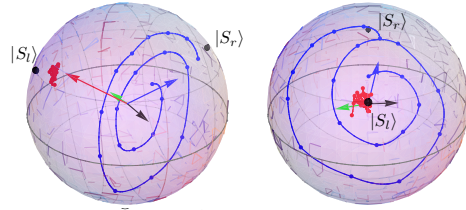
Fidelities for the $\hat{E}_i$:
$\hat{E}_1$: $F_S = 0.83$, $F_T = 0.88$, $V = 0.71$
$\hat{E}_2$: $F_S = 0.73$, $F_T = 0.84$, $V = 0.57$
$\hat{E}_3$: $F_S = 0.62$, $F_T = 0.72$, $V = 0.34$
$\hat{E}_4$: $F_S = 0.58$, $F_T = 0.76$, $V = 0.34$
The average fidelity of the triplet outcomes was 0.80.
The average fidelity of the singlet outcomes was 0.69.
The average fidelity of all measurements was 0.75.
The average visibility was 0.49.

Fig. 3.5.3 Pulse sequences for the EO qubit state tomography.

Bibliography

1. K. C. Nowack, M. Shafiei, M. Laforest, G. E. D. K. Prawiroatmodjo, L. R. Schreiber, C. Reichl, W. Wegscheider, and L. M. K. Vandersypen, *Single-Shot Correlations and Two-Qubit Gate of Solid-State Spins*, Science **333**, 1269 (2011).

2. F. H. L. Koppens, K. C. Nowack, and L. M. K. Vandersypen, *Spin echo of a single electron spin in a quantum dot*, Phys. Rev. Lett. **100**, 236802 (2008).

3. R. Brunner, Y. S. Shin, T. Obata, M. Pioro-Ladriere, T. Kubo, K. Yoshida, T. Taniyama, Y. Tokura, and S. Tarucha, *Two-Qubit Gate of Combined Single-Spin Rotation and Interdot Spin Exchange in a Double Quantum Dot*, PRL **107**, 146801 (2011).

4. M. D. Shulman, O. E. Dial, S. P. Harvey, H. Bluhm, V. Umansky, and A. Yacoby, *Demonstration of Entanglement of Electrostatically Coupled Singlet-Triplet Qubits*, Science **336**, 202 (2012).

5. S. Foletti, H. Bluhm, D. Mahalu, V. Umansky, and A. Yacoby, *Universal quantum control of two-electron spin quantum bits using dynamic nuclear polarization*, Nature Physics **5**, 903 (2009).

6. E. A. Laird, J. M. Taylor, D. P. DiVincenzo, C. M. Marcus, M. P. Hanson, and A. C. Gossard, *Coherent spin manipulation in an exchange-only qubit*, Phys. Rev. B **82** (2010).